A HIGHER-ORDER EULERIAN-LAGRANGIAN LOCALIZED ADJOINT METHOD FOR TWO-DIMENSIONAL UNSTEADY ADVECTION-DIFFUSION PROBLEMS*

Mohamed Al-Lawatia

Department of Mathematics and Statistics, Sultan Qaboos University,
P.O. Box 36, Al-Khod 123, Sultanate of Oman
Email: allawati@squ.edu.om

Abstract

We present a higher-order in-space characteristic method for the solution of the transient advection diffusion equations in two space dimensions. This method uses biquadratic trial and test functions within the framework of the Eulerian-Lagrangian localized Adjoint Methods (ELLAM). It therefore maintains the advantages of previous ELLAM schemes. Namely, it treats general boundary conditions naturally in a systematic manner, conserves mass, and symmetrizes the governing transport equations. Moreover, it generates accurate numerical solutions even if large time steps are used in the simulation. Numerical experiments are presented to illustrate the performance of this method and establish its order of convergence numerically.

Mathematics subject classification: 65D30.
Key words: Advection-diffusion equations, Characteristic methods, Eulerian-Lagrangian methods, Biquadratic interpolation.

1. Introduction

Advection-diffusion equations arise in many models in Science and Engineering and describe a wide range of natural phenomena characterized by moving fronts. In fluid dynamics, for example, the movement of a solute in groundwater is described by such an equation. These equations are known to present serious numerical difficulties especially when the magnitude of advection is relatively large. Standard finite difference and finite element methods fail to provide qualitatively correct solutions for this class of equations even with lower accuracy requirements. More specifically, these methods generate solutions which suffer from numerical artifacts including non-physical spurious oscillations and numerical diffusion that smears out sharp fronts of the solution where important chemistry and physics take place.

A number of specialized methods have been developed to resolve these difficulties. They generally can be classified as *Eulerian methods* or *characteristic methods*. Eulerian methods use fixed spatial grids and incorporate upstream weighting or some other dissipation techniques in their formulations [3, 7, 10, 11, 14, 15]. Thus, they can eliminate the non-physical oscillations present in the standard finite difference and finite element methods. Some of the Eulerian methods, such as the Godunov scheme, the total variation diminishing (TVD) schemes, and the ENO and WENO schemes, can resolve shock discontinuities from nonlinear hyperbolic conservation laws.

Characteristic methods, on the other hand, make use of the hyperbolic nature of the governing equation by utilizing tracking along the characteristics to treat the advective part of the governing equation [8,12]. These methods symmetrize the governing equations and significantly reduce the temporal truncation errors. Thus, they allow large time steps to be used in the numerical simulations without any sacrifice in accuracy, and lead to a greatly improved efficiency. However, most characteristic methods have difficulties in treating general boundary conditions and fail to conserve mass. The Eulerian-Lagrangian localized adjoint method (ELLAM) was proposed by Celia *et. al.,* [6] as an alternative characteristic formulation that alleviates the difficulties mentioned. This ELLAM formalism provides a general characteristic solution procedure for advection-diffusion equations and a consistent framework for conserving mass and treating general boundary conditions.

The original ELLAM method is for the solution of one-dimensional constant-coefficient advection-diffusion equations, in which piecewise-linear trial and test functions are used in the weak formulation. The strong potential of this method lead to the development of multidimensional ELLAM schemes using either the finite element or finite volume approaches [4,9,13,18–21]. Most of the work on ELLAM methods followed the traditional approach in which first- and second-order numerical methods are probably the most widely used in the numerical simulation to subsurface porous medium flow processes, especially in terms of characteristic methods. The main reasons for the choice of lower-order methods is the fact that most mathematical models for subsurface porous medium flows admit solutions with moving steep fronts and relatively complicated structures. As a result, the solutions of these models usually have minimal regularities. This is due to a number of factors including the strong heterogeneity of the porous media, the non linearity and close couplings between the equations in the system, the strong effect of the singular sources and sinks, the compressibility of the fluid mixture and the medium, and the enormous size of field-scale application and the required long time period of prediction. In these circumstances, higher-order numerical schemes usually cannot reach higher-order convergence rates. Nevertheless, it is well known that higher-order numerical methods have generated numerical solutions with greatly improved accuracy and resolution in the context of nonlinear hyperbolic conservation laws, despite the fact that the solutions to nonlinear conservation laws exhibit shock discontinuities, complicated structures, and minimal regularities.

Motivated by the success of higher-order methods in aerodynamics and other applications, we continue our research on the development of higher-order ELLAM schemes for the solution of transient advection-diffusion equations. We have worked on the development of higher-order-in-time ELLAM schemes with success [1, 16]. We have also considered higher-order in space ELLAM schemes in one-space dimension [2]. In this paper, we present an ELLAM scheme, for the transient advection-diffusion equation in two space dimensions, which uses higher-order bi-quadratic trial and test functions in space. The derived scheme possesses a higher-order spatial convergence rate compared to previous two-dimensional ELLAM methods and improved spatial resolution. Numerical experiments are presented to illustrate the performance of the new ELLAM scheme and to numerically verify its convergence rates, which were derived theoretically for one-dimensional problems [17].

The paper is organized in the following way. In the next section, we review the development of the ELLAM method. The details of the numerical approximation will be discussed in Section 3. Numerical results will be reported in Section 4. Some relevant discussions will be presented in the final section.

2. Development of the ELLAM Schemes

The model equation considered is the two-dimensional unsteady-state advection diffusion equation

$$\frac{\partial(\phi(\mathbf{x},t)\,u(\mathbf{x},t))}{\partial t} + \nabla \cdot \Big(\mathbf{v}(\mathbf{x},t)u(\mathbf{x},t) - \mathbf{D}(\mathbf{x},t)\nabla u(\mathbf{x},t)\Big) = f(\mathbf{x},t) \qquad (2.1)$$

where $\mathbf{x} = (x,y)$, $\nabla = \langle \partial/\partial x, \partial/\partial y \rangle$, $\phi(\mathbf{x},t)$ is the retardation coefficient, $\mathbf{v}(\mathbf{x},t)$ is the velocity field, $\mathbf{D}(\mathbf{x},t)$ is the diffusion-dispersion tensor, and $f(\mathbf{x},t)$ is a source or sink term. While the ELLAM method can be developed for any bounded spatial domain which admits a quasi-uniform triangular or rectangular partition, for simplicity of presentation we consider a spatial domain of the form $\Omega = [a,b] \times [c,d]$. To close the system, we assume that an appropriate initial condition and any proper combination of Dirichlet, Neumann, or flux boundary conditions are specified at the inflow or outflow parts of the boundary.

2.1. Partition and Characteristic Tracking

ELLAM methods, in general, can be developed for any quasi-uniform partition of the space-time domain $\Omega \times [0,T]$. However, for simplicity of presentation, we consider the following uniform rectangular partition in space and time

$$\begin{aligned}
x_i &= a + i\,\Delta x, \quad i = 0, \cdots, I \quad \text{with} \ \ \Delta x = (b-a)/I, \\
y_j &= c + j\,\Delta y, \quad j = 0, \cdots, J \quad \text{with} \ \ \Delta y = (d-c)/J, \\
t^n &= n\,\Delta t, \qquad\quad n = 0, \cdots, N \ \ \text{with} \ \ \Delta t = T/N,
\end{aligned} \qquad (2.2)$$

where I, J, and N are positive integers. The numerical scheme uses a time-stepping procedure, and so, we only need to focus on the current time interval $(t^{n-1}, t^n]$. By multiplying equation (2.1) by a piecewise smooth test function w that vanishes outside $\Omega \times (t^{n-1}, t^n]$ we obtain a weak form of Eq. (2.1)

$$\int_{\Omega} (\phi\,u)(\mathbf{x},t^n)\,w(\mathbf{x},t^n)\,d\mathbf{x} + \int_{t^{n-1}}^{t^n} \int_{\Omega} (\mathbf{D}\nabla u) \cdot \nabla w\,d\mathbf{x}\,dt$$

$$- \int_{t^{n-1}}^{t^n} \int_{\Omega} u\left(\phi\,\frac{\partial w}{\partial t} + \mathbf{v} \cdot \nabla w\right) d\mathbf{x}\,dt + \int_{t^{n-1}}^{t^n} \int_{\partial\Omega} (\mathbf{v}\,u - \mathbf{D}\nabla u)\,w \cdot \mathbf{n}\,dS$$

$$= \int_{\Omega} (\phi\,u)(\mathbf{x},t^{n-1})\,w(\mathbf{x},t^{n-1}{}_+)\,d\mathbf{x} + \int_{t^{n-1}}^{t^n} \int_{\Omega} f\,w\,d\mathbf{x}\,dt, \qquad (2.3)$$

where $w(\mathbf{x},t^{n-1}{}_+) = \lim_{t \to t^{n-1}} w(\mathbf{x},t)$ which takes into account the fact that w is discontinuous in time at time t^{n-1}.

In the ELLAM framework [6], the test functions $w(\mathbf{x},t)$ in equation (2.3) are selected to satisfy, within the tolerance of the accuracy desired, the homogeneous equation of the hyperbolic part of the adjoint equation of (2.1)

$$\phi\,\frac{\partial w}{\partial t} + \mathbf{v} \cdot \nabla w = 0 \qquad (2.4)$$

to reflect the Lagrangian nature of Eq. (2.1); in other words, the test functions should be chosen to be constant along the characteristics. These characteristic curves of Eq. (2.1) are defined as

solutions to initial value problems for the ordinary differential equation

$$\frac{d\mathbf{x}}{dt} = \mathbf{v}_\phi(\mathbf{x}, t) := \left(\frac{\mathbf{v}(\mathbf{x}, t)}{\phi(\mathbf{x}, t)}\right). \tag{2.5}$$

However, solving this equation for a generic velocity field is not possible, in general. Thus, we need to use some numerical means to track the characteristics approximately. A variety of algorithms may be used for that purpose, including the Euler and Runge-Kutta methods. In our formulations we use a second order Runge-Kutta method and define the approximate characteristic curve $X(\theta; \bar{\mathbf{x}}, \bar{t})$ emanating from a point $(\bar{\mathbf{x}}, \bar{t})$ by

$$X(\theta; \bar{\mathbf{x}}, \bar{t}) = \bar{\mathbf{x}} + \frac{\theta - \bar{t}}{2}\left(\mathbf{v}_\phi(\bar{\mathbf{x}}, \bar{t}) + \mathbf{v}_\phi(\bar{\mathbf{x}} - (\theta - t)\mathbf{v}_\phi(\bar{\mathbf{x}}, \bar{t}), \bar{t})\right). \tag{2.6}$$

Here θ is the time position along that characteristic. Moreover, to further improve the accuracy of tracking, we divide the global step Δt into a number of micro time steps, and the tracking described by Eq. (2.6) can be carried across these micro steps.

2.2. The Reference Equation

The family of ELLAM methods can be formulated by evaluating the space-time integrals in Eq. (2.3) along the approximate characteristics. Special attention needs to be given to the two triple integrals in this weak form: the second (source and sink) term on the right-hand side of the equation and the second (diffusion) term on the left-hand side. These integrals, in a similar way to all other terms, are changed to the characteristic variables, and then a backward Euler quadrature along the characteristics is applied. This results in the following formulation for the ELLAM schemes,

$$\int_\Omega \phi(\mathbf{x}, t^n)\, u(\mathbf{x}, t^n)\, w(\mathbf{x}, t^n)\, d\mathbf{x} + \int_\Omega \Delta t^{(I)}(\mathbf{x})(\mathbf{D}\nabla u)(\mathbf{x}, t^n) \cdot \nabla w(\mathbf{x}, t^n)\, d\mathbf{x}$$

$$+ \int_{t^{n-1}}^{t^n} \int_{\partial\Omega^{(O,n)}} \Delta t^{(O)}(\mathbf{x}, t)(\mathbf{D}\nabla u) \cdot \nabla w\, (\mathbf{v} \cdot \mathbf{n})\, dS$$

$$- \int_{t^{n-1}}^{t^n} \int_\Omega u \left(\phi\, \frac{\partial w}{\partial t} + \mathbf{v} \cdot \nabla w\right) d\mathbf{x}\, dt + \int_{t^{n-1}}^{t^n} \int_{\partial\Omega} (\mathbf{v}u - \mathbf{D}\nabla u) \cdot \mathbf{n}\, w\, dS$$

$$= \int_\Omega \phi(\mathbf{x}, t^{n-1})\, (\mathbf{x}, t^{n-1})\, w(\mathbf{x}, t^{n-1}{}_+)\, d\mathbf{x} + \int_\Omega \Delta t^{(I)} f(\mathbf{x}, t^n)\, w(\mathbf{x}, t^n)\, d\mathbf{x}$$

$$+ \int_{t^{n-1}}^{t^n} \int_{\partial\Omega^{(O,n)}} \Delta t^{(O)}(\mathbf{x}, t) f\, w\, (\mathbf{v} \cdot \mathbf{n})\, dS + \mathcal{E}(u, w) \tag{2.7}$$

where $\partial\Omega^{(O,n)}$ is the outflow part of the boundary, $\mathcal{E}(u, w)$ is the truncation error due to the use of Euler quadrature, $\Delta t^{(I)}\mathbf{x} = t^n - t^*(\mathbf{x})$ where $t^*(\mathbf{x})$ is the time instance when the characteristic emanating from $(\mathbf{x}, t^n)$ intersects the boundary $\partial\Omega \times [t^{n-1}, t^n]$, and similarly $\Delta t^{(O)}(\mathbf{x}, t) = t - t^*(\mathbf{x}, t)$, where $t^*(\mathbf{x}, t)$ is the time instance when the characteristic emanating from $(\mathbf{x}, t)$ intersects the boundary; both time steps extend to Δt when the corresponding characteristics do not intersect the boundary.

3. Numerical Approximation

The numerical schemes can use arbitrarily high-order trial and test functions. Here we present the schemes using piecewise bilinear and biquadratic basis functions over rectangular elements determined by partition (2.2). The original one dimensional Linear ELLAM scheme uses the hat functions

$$
l_i(x, t^n) = \begin{cases} \dfrac{x - x_{i-1}}{\Delta x}, & \text{if } x \in [x_{i-1}, x_i] \\[2mm] \dfrac{x_{i+1} - x}{\Delta x}, & \text{if } x \in [x_i, x_{i+1}] \\[2mm] 0, & \text{otherwise} \end{cases} \tag{3.1}
$$

as basis functions [6]. The two-dimensional bilinear ELLAM scheme is the natural extension which uses two-dimensional piecewise bilinear polynomials that are formed by taking direct products of associated one dimensional basis functions (3.1). That is, if $l_i(x, t^n)$ is the piecewise linear function defined along x at the grid point x_i, and $l_j(y, t^n)$ is the corresponding function along y at the grid point y_j, then the piecewise bilinear basis function associated with node k located at the grid point (x_i, y_i) is defined by $w_k(\mathbf{x}, t^n) = l_i(x, t^n)\, l_i(y, t^n)$ (see Fig. 3.1(a)).

(a)   (b)
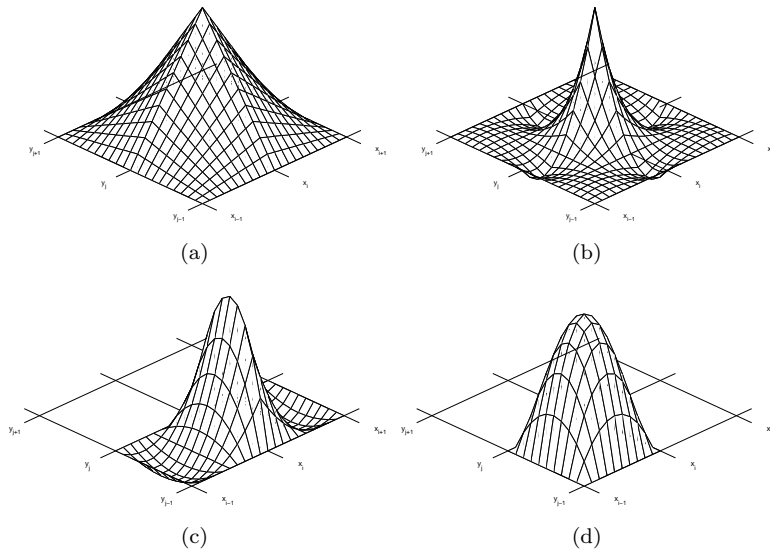
(c)   (d)

Fig. 3.1. Representative global basis functions at time t^n for (a) bilinear, (b) biquadratic interpolation. Only nonzero parts are plotted.

In a similar manner, we can present the basis functions of the higher-order (biquadratic) ELLAM by considering the piecewise quadratic basis functions in one-space dimension

$$
l_{2i}(x, t^n) = \begin{cases} \dfrac{2(x - x_{i-1})(2 - x_{i-1} - x_i)}{(\Delta x)^2}, & x \in [x_{i-1}, x_i] \\[3mm] \dfrac{2(x - x_{i+1})(2 - x_{i+1} - x_i)}{(\Delta x)^2}, & x \in [x_i, x_{i+1}] \\[3mm] 0, & \text{otherwise,} \end{cases} \tag{3.2}
$$

$$l_{2i+1}(x, t^n) = \begin{cases} \dfrac{4(x - x_i)(x_{i+1} - x)}{(\Delta x)^2}, & x \in [x_i, x_{i+1}] \\ \\ 0, & \text{otherwise.} \end{cases}$$

The two-dimensional basis functions are then defined to be the direct product of these one dimensional functions. A representative corner-node, midside-node, and center-node biquadratic basis functions are presented in Fig. 3.1. These methods use similar basis functions at the outflow boundary of the space-time domain. Here we recall that on the interior of the domain, these test functions extend to be constant along the approximate characteristics. The two EL-LAM schemes are based on approximating the exact solution u of Eq. (2.1) (or equivalently the reference Eq. (2.7)) by a piecewise bilinear or biquadratic trial function U, of the same degree as the test functions. Incorporating the trial and test functions above into the reference Eq. (2.7) and dropping the truncation error term $\mathcal{E}(u, w)$ and the adjoint term, the fourth term on the left side of the equation, gives the corresponding ELLAM schemes

$$\int_\Omega \phi(\mathbf{x}, t^n)\, U(\mathbf{x}, t^n)\, w(\mathbf{x}, t^n)\, d\mathbf{x} + \int_\Omega \Delta t^{(I)}(\mathbf{x})(\mathbf{D}\nabla U)(\mathbf{x}, t^n) \cdot \nabla w(\mathbf{x}, t^n)\, d\mathbf{x}$$

$$+ \int_{t^{n-1}}^{t^n} \int_{\partial\Omega^{(O,n)}} \Delta t^{(O)}(\mathbf{x}, t)(\mathbf{D}\nabla U) \cdot \nabla w\, (\mathbf{v} \cdot \mathbf{n})\, dS$$

$$+ \int_{t^{n-1}}^{t^n} \int_{\partial\Omega} (\mathbf{v}U - \mathbf{D}\nabla U) \cdot \mathbf{n}\, w\, dS \qquad (3.3)$$

$$= \int_\Omega \phi(\mathbf{x}, t^{n-1})\, (\mathbf{x}, t^{n-1})\, w(\mathbf{x}, t^{n-1}_+)\, d\mathbf{x} + \int_\Omega \Delta t^{(I)} f(\mathbf{x}, t^n)\, w(\mathbf{x}, t^n)\, d\mathbf{x}$$

$$+ \int_{t^{n-1}}^{t^n} \int_{\partial\Omega^{(O,n)}} \Delta t^{(O)}(\mathbf{x}, t) f\, w\, (\mathbf{v} \cdot \mathbf{n})\, dS.$$

With the known solution $U(\mathbf{x}, t^{n-1})$ from the computations at the previous time step t^{n-1} (or the initial condition) and the prescribed boundary conditions, each ELLAM method solves for $U(\mathbf{x}, t^n)$ with $\mathbf{x}$ in Ω and also for $(\mathbf{x}, t)$ for points in $\Omega^{(O,n)}$. These schemes symmetrize the governing Eq. (2.1), generate accurate numerical solutions even if large time steps are used, and conserve mass [6].

4. Numerical Experiments

We conduct several example runs to observe the performance of the bilinear and biquadratic ELLAM methods (L-ELLAM, Q-ELLAM) developed and to numerically verify their convergence rates which were proved for the one-dimensional case in [17].

4.1. Convergence Rates

In this example, we establish the convergence rates in space of the higher-order (biquadratic) ELLAM scheme as well as the bilinear ELLAM method. As a model problem, we consider the transport of a rotating Gaussian pulse with initial configuration given by

$$u_0(x, y) = \exp\left(-\frac{(x - x_c)^2 + (y - y_c)^2}{2\sigma^2}\right) \qquad (4.1)$$

Table 4.1: Order of convergence in space of the L-ELLAM and Q-ELLAM methods for the transport of the Gaussian pulse problem

METHOD	h	Δt	$\mathcal{L}_2$ Error	$\mathcal{L}_1$ Error	CPU seconds
L-ELLAM	1/21	$\pi/200$	1.88270×10^{-2}	4.69993×10^{-3}	80.50
	1/22	$\pi/200$	1.76360×10^{-2}	4.26819×10^{-3}	90.08
	1/23	$\pi/200$	1.64753×10^{-2}	3.89080×10^{-3}	98.10
	1/24	$\pi/200$	1.53485×10^{-2}	3.51173×10^{-3}	104.42
	1/25	$\pi/200$	1.42735×10^{-2}	3.20672×10^{-3}	115.13
	1/26	$\pi/200$	1.33057×10^{-2}	2.91680×10^{-3}	125.55
	1/27	$\pi/200$	1.23982×10^{-2}	2.65664×10^{-3}	129.96
	1/28	$\pi/200$	1.16136×10^{-2}	2.41584×10^{-3}	138.64
	1/29	$\pi/200$	1.08832×10^{-2}	2.22009×10^{-3}	149.35
	1/30	$\pi/200$	1.02231×10^{-2}	2.04316×10^{-3}	159.74
			$\alpha = 1.8$	$\alpha = 2.3$	
			$C_\alpha = 3.21$	$C_\alpha = 5.37$	
Q-ELLAM	1/21	$\pi/200$	2.50893×10^{-3}	4.17767×10^{-4}	111.80
	1/22	$\pi/200$	2.18695×10^{-3}	3.53850×10^{-4}	123.88
	1/23	$\pi/200$	1.88490×10^{-3}	3.01452×10^{-4}	132.87
	1/24	$\pi/200$	1.58538×10^{-3}	2.47161×10^{-4}	146.37
	1/25	$\pi/200$	1.35704×10^{-3}	2.06903×10^{-4}	160.17
	1/26	$\pi/200$	1.17361×10^{-3}	1.78075×10^{-4}	164.75
	1/27	$\pi/200$	1.06855×10^{-3}	1.60205×10^{-4}	177.68
	1/28	$\pi/200$	9.83897×10^{-4}	1.46533×10^{-4}	200.01
	1/29	$\pi/200$	9.42515×10^{-4}	1.38701×10^{-4}	204.11
	1/30	$\pi/200$	9.00645×10^{-4}	1.29302×10^{-4}	218.41
			$\alpha = 3.0$	$\alpha = 3.4$	
			$C_\alpha = 26.65$	$C_\alpha = 13.0$	

where the center and the standard deviation are $(x_c, y_c) = (0, -0.25)$ and $\sigma = 0.0316$. Eq. (2.1) is solved with this initial condition over a domain of $\Omega = [-0.5, 0.5] \times [-0.5, 0.5]$ for a period of $T = \pi/2$. The rotating velocity field is $\mathbf{v}(x, y, t) = \langle -4y, 4x \rangle$ and the diffusion tensor $\mathbf{D} = 0.0002\mathbf{I}_2$ (where $\mathbf{I}_2$ is the 2×2 identity matrix). To complete the model, we select $\phi = 1$ and consider a zero source/sink term. The exact solution to this problem is given by

$$u(x, y, t) = \frac{2\sigma^2}{2\sigma^2 + 4(0.0002)t} \exp\left(-\frac{(\bar{x} - x_c)^2 + (\bar{y} - y_c)^2}{2\sigma^2 + 4(0.0002)t}\right). \tag{4.2}$$

where $(\bar{x}, \bar{y}) = (x \cos 4t + y \sin 4t, -x \sin 4t + y \cos 4t)$.

The truncation error of the two ELLAM schemes can be estimated as follows

$$\max_{n=0,..,N} \|u(\mathbf{x}, t^n) - U(\mathbf{x}, t^n)\|_{\mathcal{L}_P} \leq C_\alpha(h)^\alpha + C_\beta(\Delta t)^\beta \tag{4.3}$$

in the $\mathcal{L}_2$ and the $\mathcal{L}_1$ norms where $\Delta x = \Delta y =: h$; here α and β are the orders of convergence in space and time, respectively [17]. Because the temporal convergence rates of ELLAM schemes using a backward Euler step in time were previously reported for one-dimensional problems in [1, 16], in this example we only measure the spatial convergence rates of the bilinear and biquadratic ELLAM methods. We vary the spatial grid size h systematically with the temporal step being sufficiently refined so that the temporal errors are negligible. We then use a linear regression to fit the spatial convergence rates. Table 4.1 contains the $\mathcal{L}_2$ and the $\mathcal{L}_1$ norms of

Table 4.2: Results of the L-ELLAM and Q-ELLAM methods for the transport of the box function problem

METHOD	h	Δt	$\mathcal{L}_2$ Error	$\mathcal{L}_1$ Error	CPU seconds
L-ELLAM	1/85	$\pi/12$	2.12625×10^{-3}	4.93197×10^{-4}	45.76
	1/85	$\pi/60$	1.69367×10^{-3}	3.78598×10^{-4}	227.67
	1/90	$\pi/24$	5.36936×10^{-4}	1.23854×10^{-4}	112.03
	1/90	$\pi/60$	4.91244×10^{-4}	1.23542×10^{-4}	283.73
Q-ELLAM	1/85	$\pi/12$	2.62226×10^{-3}	6.21217×10^{-4}	97.67
	1/85	$\pi/60$	1.66480×10^{-3}	3.68038×10^{-4}	322.47
	1/90	$\pi/24$	1.05805×10^{-3}	2.79854×10^{-4}	201.62
	1/90	$\pi/60$	4.77819×10^{-4}	1.23959×10^{-4}	410.70

the errors generated in runs carried out for the L-ELLAM and Q-ELLAM, respectively. These results verify the optimal-order convergence rates of these ELLAM schemes in the two norms. We also remark that the constant C_α increases as the degree of the trial and test functions increases. This is because the errors for higher-order ELLAM schemes depend on higher-order Sobolev norms of the exact solution.

The choice of the relatively small time steps Δt in Table 4.1 was to establish the order of convergence. However, one main advantage of ELLAM and characteristic methods in general is that they allow large time steps in the simulations. Therefore, in Fig. 4.1, we present the solutions generated by both ELLAM methods for this model problem using a grid of size $h = 1/60$ and the relatively larger $\Delta t = \pi/30$. Both L-ELLAM and Q-ELLAM perform very well and present a solution with relatively small errors of 4.50754×10^{-4} and 2.58679×10^{-4} in the $\mathcal{L}_2$ norm, respectively, and 6.65402×10^{-4} and 3.72599×10^{-4} in the $\mathcal{L}_1$ norm with a CPU real time of 56.55 and 65.9 seconds.

4.2. Transport of a Diffused Box Function

In order to test the L-ELLAM and Q-ELLAM methods for problems with discontinuous data, we consider in this example the transport of a diffused rectangular box function with initial configuration given by

$$u_o(x,y) = \begin{cases} 1, & (x,y) \in [-0.1, 0.1] \times [-0.35, -0.15] \\ 0, & \text{otherwise} \end{cases} \tag{4.4}$$

subject to Eq. (2.1). The parameters selected in this model problem are the same as those in the previous example and so is the space-time domain. The exact solution of this model problem is given by

$$u(x,y,t) = \frac{1}{4}\left[\text{erf}\left(\frac{\bar{x}+0.1}{\sqrt{0.0008t}}\right) - \text{erf}\left(\frac{\bar{x}-0.1}{\sqrt{0.0008t}}\right)\right] \times$$

$$\left[\text{erf}\left(\frac{\bar{y}+0.35}{\sqrt{0.0008t}}\right) - \text{erf}\left(\frac{\bar{y}+0.15}{\sqrt{0.0008t}}\right)\right] \tag{4.5}$$

where $\text{erf}(x) = 2/\sqrt{\pi}\int_0^x e^{-s^2}ds$ is the standard error function and $(\bar{x}, \bar{y}) = (x\cos(4t) + y\sin(4t), -x\sin(4t) + y\cos(4t))$ as defined before.

In Table 4.2 we present the numerical results of some representative example runs, while in Fig. 4.2, we present plots of the solutions of the L-ELLAM and Q-ELLAM schemes using a
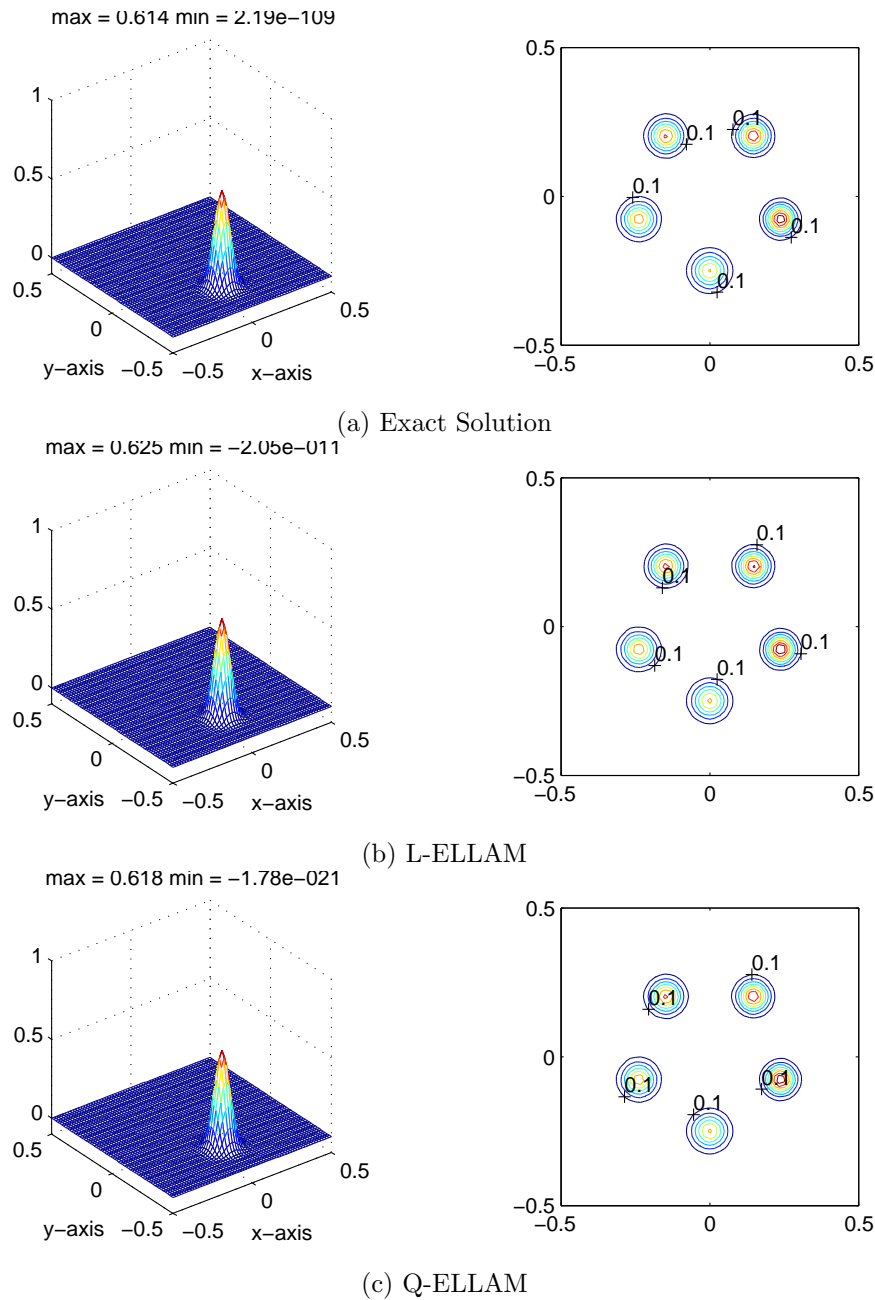
max = 0.614 min = 2.19e−109

(a) Exact Solution

max = 0.625 min = −2.05e−011

(b) L-ELLAM

max = 0.618 min = −1.78e−021

(c) Q-ELLAM

Fig. 4.1. Plots at $t = \pi/2$ and contours at $t = \pi/10$, $\pi/5$, $3\pi/10$, $2\pi/5$, $\pi/2$ of the exact solution and the solutions of L-ELLAM and Q-ELLAM with $h = 1/60$ and $\Delta t = \pi/30$ for the transport of the Gaussian pulse problem

grid of sizes $h = 1/60$ and $\Delta t = \pi/30$ as well as the exact solution. These results show that the ELLAM schemes very accurately capture the details and the steep fronts of the exact solution, with the Q-ELLAM performing better. These results support the development of higher-order schemes. On the other hand, these results also call for the development of higher-order ELLAM schemes with rigorous higher-order temporal approximations (e.g., TVD in time). This will be one of the objectives for our future work.

(a) Exact Solution
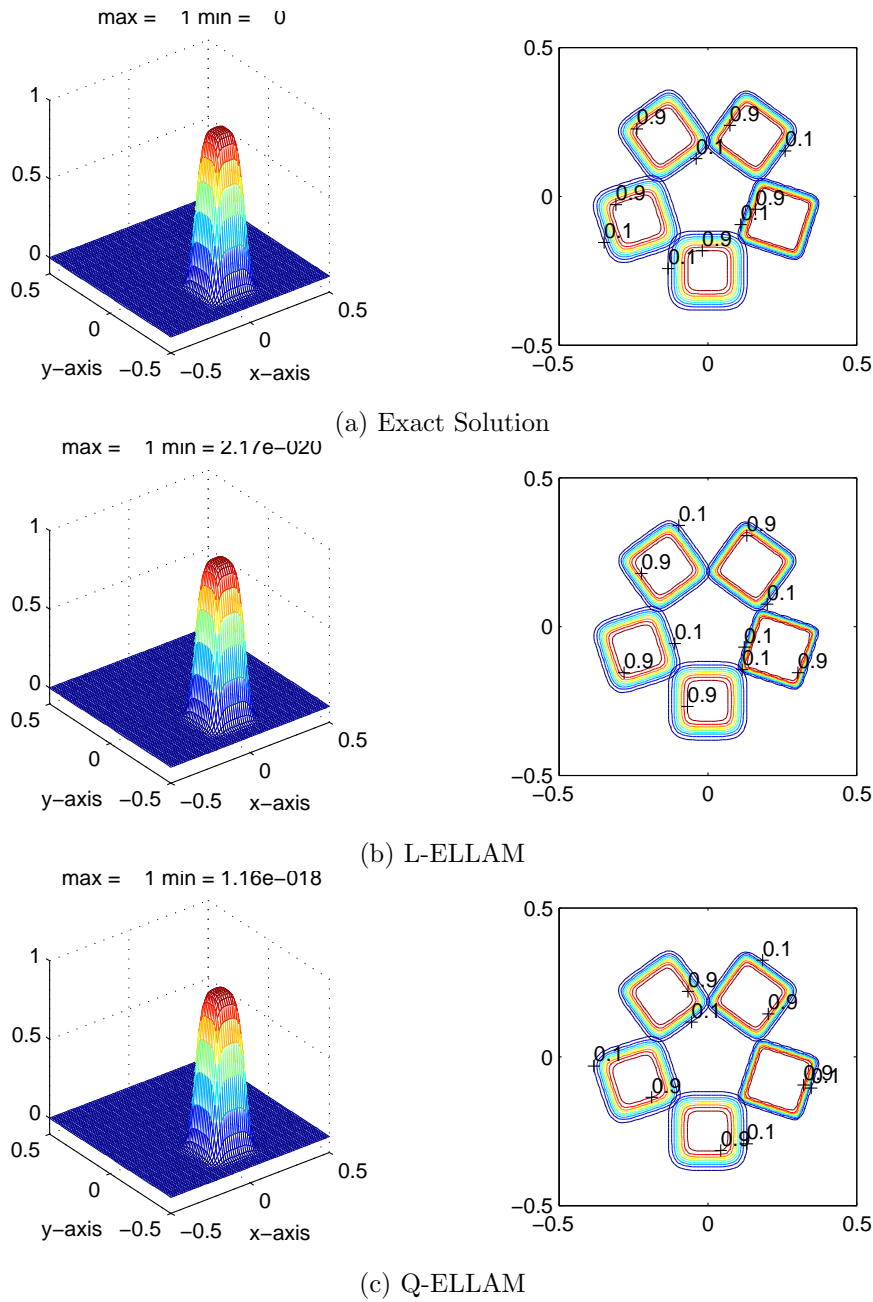

(b) L-ELLAM

(c) Q-ELLAM

Fig. 4.2. Plots at $t = \pi/2$ and contours at $t = \pi/10, \pi/5, 3\pi/10, 2\pi/5, \pi/2$ of the exact solution and the solutions of L-ELLAM and Q-ELLAM with $h = 1/60$ and $\Delta t = \pi/30$ for the transport of the box function problem

4.3. Diffusion in a plane shear flow

The next set of numerical experiments involves the transport of a point source under the influence of a shear flow [5]. The model Eq. (2.1) is solved using a velocity field of $\mathbf{v}(x, y, t) = \langle 1 + 2y, 0 \rangle$ and a diffusion of $\mathbf{D} = 0.0001\mathbf{I}_2$ over a spatial domain of $[0, 1.3] \times [-0.2, 0.2]$. The analytic solution subject to an initial condition of $M\delta(x_0, 0)$ (where δ represents the dirac delta

(a) Exact Solution
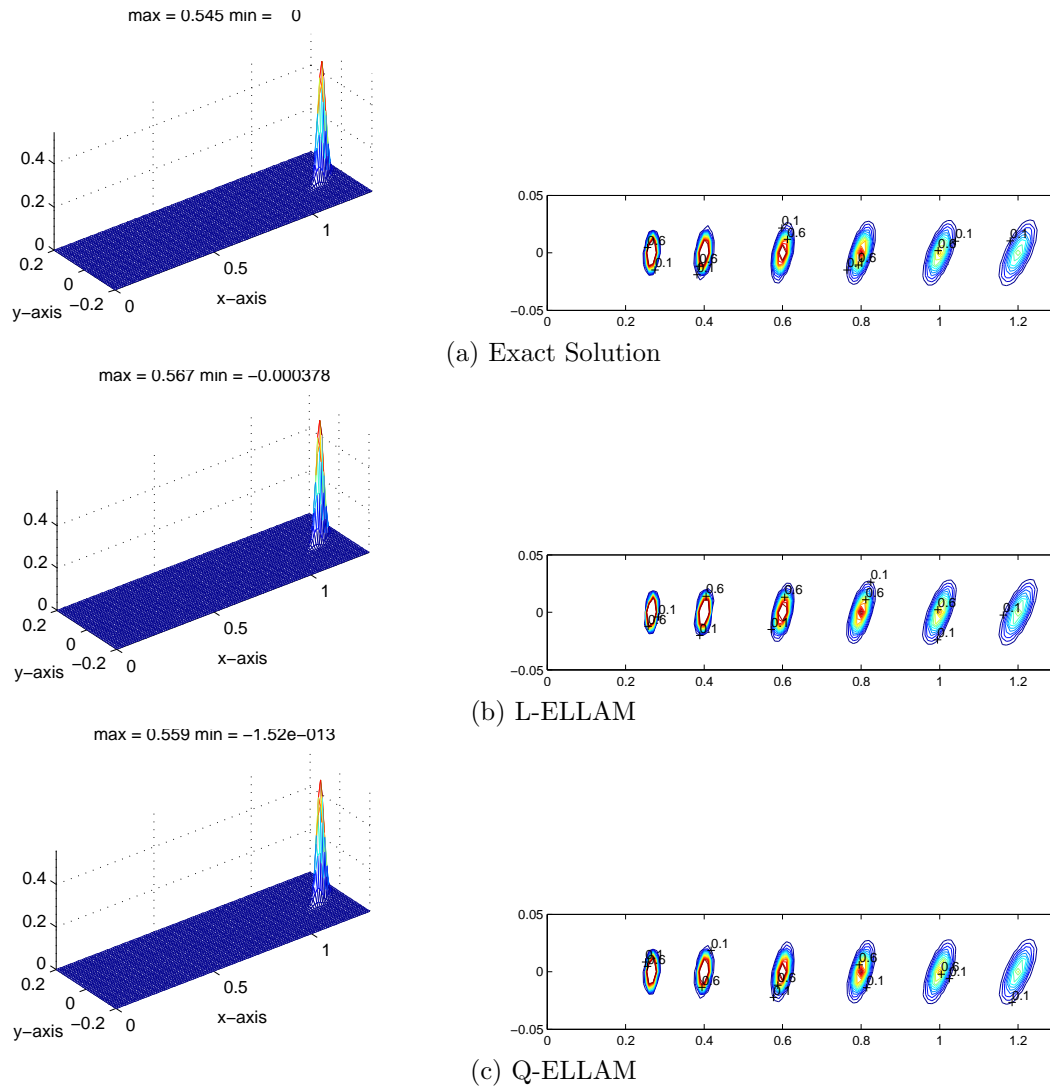

(b) L-ELLAM

(c) Q-ELLAM

Fig. 4.3. Plots of the solution at $t = 1.2$ and contours at $t = 0.2, 0.4, 0.6, 0.8, 1.0$ 1.2 of the exact solution and the solutions of L-ELLAM and Q-ELLAM with $h = 1/100$ and $\Delta t = 1/15$ for the diffusion in a plane shear flow problem

function) is given by

$$u(x, y, t) = \frac{M}{0.0004\pi t \sqrt{1 + \frac{4t^2}{12}}} \exp\left(-\frac{(x - x_0 - t - yt)^2}{0.0004t(1 + \frac{4t^2}{12})} - \frac{y^2}{0.0004t}\right). \tag{4.6}$$

In the model problem we work with a finite initial condition at $t = 0.2$ and simulate over the time interval $[0.2, 1.2]$ using $M = 0.001$.

As a representative model run, we simulate the problem with a discretization of $\Delta x = \Delta y = 1/100$ and $\Delta t = 1/15$ and present the L-ELLAM and Q-ELLAM solutions in Fig. 4.3. The norms of the absolute errors generated are an $\mathcal{L}_2$ norm of 8.54250×10^{-4} and an $\mathcal{L}_1$ norm of 5.41365×10^{-5} for the L-ELLAM using 73.61 CPU seconds and an $\mathcal{L}_2$ norm of 4.91267×10^{-4} and an $\mathcal{L}_1$ norm 3.52839×10^{-5} consuming 104.48 CPU seconds.

5. Discussion

In this paper we have presented a characteristic scheme of a high order in space to solve the two-dimensional advection diffusion equation. This method uses piecewise biquadratic test and trial functions over rectangular grids within a finite element framework of the Eulerian-Lagrangian localized adjoint methods (ELLAM). The derived scheme maintains the advantages of the class of ELLAM schemes which include global mass conservation and a natural treatment of the boundary conditions in the formulation. Moreover, it is not subject to CFL restrictions, and thus allows for large time steps to be used in the simulation without any sacrifice to accuracy.

Numerical experiments are presented which investigate the performance of the method developed and its convergence rates in comparison to previously developed ELLAM methods based on linear interpolation. These results verify the higher order convergence rate in space expected from the order of polynomial interpolation used. Moreover, they illustrate the strong potential of the derived scheme and show a promising for practical use and a wide industrial applicability. To further improve the accuracy and convergence behaviour of the method, one could consider coupling the higher-order discretization in space with a high-order approximation in time (e.g., TVD in time). This will be a topic for future investigation.

References

[1] M. Al-Lawatia, R.C. Sharpley, and H. Wang, Second-order characteristics methods for advection-diffusion equations and comparison to other schemes, *Adv. Water Resour.*, **22** (1999), 741-768.

[2] M. Al-Lawatia, H. Wang, A family of higher-order Eulerian-Lagrangian localized adjoint methods for advection-diffusion equations, *Contemp. Math.*, **295** (2002), 25-35.

[3] E.T. Bouloutas and M.A. Celia, An improved cubic Petrov-Galerkin method for simulation of transient advection-diffusion processes in rectangularly decomposable domains, *Comput. Methods Appl. Mech. Engrg.*, **91** (1991), 289-308.

[4] P.J. Binning, and M.A. Celia, A forward particle tracking Eulerian-Lagrangian localized adjoint method for solution of the contaminant transport equation in three dimensions, *Adv. Water Resour.*, **25** (2002), 147-157.

[5] H. Carter and A. Okubo, A study of the physical processes of movement and dispersion in the Cape Kennedy area, Chesapeake Bay Inst. Ref 65-2, Johns Hopkins Univ., Baltimore, MD, 1965.

[6] M.A. Celia, T.F. Russell, I. Herrera, and R.E. Ewing, An Eulerian-Lagrangian localized adjoint method for the advection-diffusion equation, *Adv. Water Resour.*, **13** (1990), 187-206.

[7] C.N. Dawson, Godunov-mixed methods for advective flow problems in one space dimension, *SIAM J. Numer. Anal.*, **28** (1991),1282-1309.

[8] J. Douglas, Jr. and T.F. Russell, Numerical methods for convection-dominated diffusion problems based on combining the method of characteristics with finite element or finite difference procedures, *SIAM J. Numer. Anal.*, **19** (1982), 871-885.

[9] C. I. Heberton, T.F. Russell, L.F. Konikow, and G.Z. Hornberger, A three-dimensional finite-volume Eulerian-Lagrangian localized adjoint method (ELLAM) for solute-transport modeling, USGS water-resources invstigation report 00-4087, Reston, Virginia, 2000.

[10] T.J.R. Hughes and M. Mallet, A new finite element formulation for computational fluid dynamics III, The general Streamline operator for multidimensional advective-diffusive systems, *Comput. Methods Appl. Mech. Engrg.*, **58** (1986), 305–328.

[11] C. Johnson, Numerical Solution of Partial Differential Equations by the Finite Element Method, Cambridge University Press, Cambridge, 1987.

[12] O. Pironneau, On the transport-diffusion algorithm and its application to the Navier-Stokes equations, *Numer. Math.*, **38** (1982), 309-33.

[13] T.F. Russell and R.V. Trujillo, Eulerian-Lagrangian localized adjoint methods with variable coefficients in multiple dimensions, in: Gambolati, *et al.* (eds.), Computational Methods in Surface Hydrology 357–363, Springer-Verlag, Berlin, 1990.

[14] X.-D. Liu, S. Osher, and T. Chan, Weighted essentially nonoscillatory schemes, *J. Comput. Phys.*, **115** (1994), 200–212.

[15] B. van Leer, On the relation between the upwind-differencing schemes of Godunov, Engquist-Osher and Roe, *SIAM J. Sci. Comput.*, **5** (1984), 1-20.

[16] H. Wang, M. Al-Lawatia, and A.S. Telyakovskiy, A Runge-Kutta characteristic method for first-order linear hyperbolic equations, *Numer. Methods Partial Differential Equations*, **13** (1997), 617-661.

[17] H. Wang, A family of ELLAM schemes for advection-diffusion-reaction equations and their convergence analyses, *Numer. Methods Partial Differential Equations*, **14** (1998), 739-780.

[18] H. Wang, R.E. Ewing, G. Qin, S.L. Lyons, M. Al-Lawatia, S. Man, A family of Eulerian-Lagrangian localized adjoint methods for multi-dimensional advection-reaction equations, *J. Comput. Phys.*, **152** (1999), 120–163.

[19] H. Wang, H., H.K. Dahle, R.E. Ewing, M.S. Espedal, R.C. Sharpley, and S. Man, An ELLAM scheme for advection-diffusion equations in two dimensions, *SIAM J. Sci. Comput.*, **20** (1999), 2160-2194.

[20] H. Wang, An optimal-order error estimate for an ELLAM scheme for two-dimensional linear advection-diffusion equations, *SIAM J. Numer. Anal.*, **37** (2000), 1338-1368.

[21] L. Wu and K. Wang, A single-node characteristic collocation method for unsteady-state convection-diffusion equations in three-dimensional spaces, *Numer. Methods Partial Differential Equations*, **27** (2011), 786–802.